Polarized emission in polariton condensates: Switching in a one-dimensional natural trap versus inversion in two dimensions

J. Cuadra* and D. Sarkar
Departamento de Física de Materiales, Universidad Autónoma de Madrid, E-28049 Madrid, Spain

L. Viña
Departamento de Física de Materiales, Universidad Autónoma de Madrid, E-28049 Madrid, Spain
Instituto de Ciencia de Materiales "Nicolás Cabrera," Universidad Autónoma de Madrid, E-28049 Madrid, Spain
and Instituto de Física de Materia Condensada, Universidad Autónoma de Madrid, E-28049 Madrid, Spain

J. M. Hvam
DTU Fotonik, Tech. Univ. Denmark, Orsteds Plads 343, DK-2800 Kgs. Lyngby, Denmark

A. Nalitov, D. Solnyshkov, and G. Malpuech
LASMEA, UMR 6602 CNRS, Université Blaise Pascal, 24 av. des Landais, 63177 Aubière, France
(Received 18 July 2013; published 26 December 2013)

We perform polarization resolved spectroscopy of two- and one-dimensional microcavity-polariton condensates, which are formed by exciting the system in the optical parametric oscillator configuration. We observe polarization inversion for linearly polarized pumping parallel to the wire in both the 1D and 2D systems. As the polarization plane of the pump is rotated, the degree of linear polarization of the 2D system oscillates between orthogonal polarizations with the same period as that of the pump. However, the 1D system switches abruptly between two states of high degree of linear polarization with half the period. Two complementary models, based on semiclassical Boltzmann kinetic equations and the Gross-Pitaevskii equation, respectively, obtain an excellent agreement with the experimental results, providing a deep insight into the mechanisms responsible for the polarization switching.

DOI: 10.1103/PhysRevB.88.235312 PACS number(s): 78.67.−n, 71.36.+c, 72.25.Rb, 42.65.Yj

I. INTRODUCTION

Microcavity exciton-polaritons are composite bosons that result from the strong coupling between a confined electromagnetic field in a microcavity and bound electron-hole pairs in an embedded quantum well. Since the first experimental evidence of strong coupling in microcavities 20 years ago,[1] and the subsequent realization of macroscopic coherent polariton condensates[2] there has been an extensive activity devoted to the rich phenomenology found in such systems including vortices,[3,4] fluid dynamics,[5] and solitons.[6,7]

The excitonic component of the quasiparticle allows polariton-polariton scattering due to Coulomb interactions. Efficient optical parametric oscillator (OPO) behavior can be achieved due to the particular shape of the polariton dispersion. Pumping the microcavity resonantly close to the inflection point of the lower polariton branch (LPB), one injects polaritons at a given wave vector and energy, which scatter, due to the strong nonlinearity present in the system, into signal and idler states conserving energy and momentum.[8,9] A nonlinear increase of the signal-state population for excitation power densities above a threshold value leads finally to condensation at the signal state.[9,10]

In microcavities with reduced dimensionality, the additional confinement produces multiple photonic modes and therefore the polariton dispersion shows multiple branches as well. Coupling between the additionally quantized photonic states with the exciton modes has been demonstrated in μm-wide, etched photonic wires.[11] In microcavity wires, different types of OPO processes have been realized.[12,13] The phase-matching conditions are not so restrictive as in the case of planar microcavities allowing parametric scattering between different branches in the sub-LPB's, between the upper and the lower branches, and even parametric processes when the cavity is pumped normally, conserving either energy[12] or momentum.[13] A recent study reviews the polaritonic mode structure of 1D systems and focuses on their power dependence for different polariton-exciton detunings.[14]

Polaritons are promising candidates for novel optical devices due to their spin structure, consisting in two spin projections on the structure growth axis. Their spin dynamics was studied for nonresonant pumping[15,16] and for the OPO process.[17–19] Other spin dependent phenomena have been proposed and demonstrated experimentally.[20–25] For possible future devices that might exploit spin properties, room-temperature operation is a further requirement. In this context, polariton lasing has been achieved in GaN-based microcavities.[26]

An inversion of the linear polarization (90° rotation) of the 2D-OPO signal with respect to the polarization of the pump has been reported previously.[19] This was explained in terms of the *negative* ratio of the scattering cross-sections of polaritons with opposite and parallel spins, which are dominated by exchange interaction. Rotation of the linear polarization as well as conversion from linear to circular polarization have been observed in Ref. 27. These results were modeled taking into account the existence of a TE-TM splitting,[28] the self-induced Larmor precession, due to the splitting between the spin-up and

spin-down polaritons, and polariton-polariton interactions. In 1D-microcavities, an inversion of the linear polarization of the signal and idler with respect to that of the pump, in interband parametric scattering processes, has been reported,[13,29] but only for particularly selected polarization conditions of the excitation.

A key hypothesis made usually in the literature to theoretically describe these phenomena is that the splitting between polarization eigenmodes is small. Two polarization eigenstates are modeled as a single state of given energy subject to an effective magnetic field, which induces rotation of the polariton pseudospin. This approach neglects that the scattering rates toward the split states are slightly different, and in fact the description breaks down if the polarization splitting is large. This is in general the case in 1D systems where the splitting between longitudinal and transverse modes is comparable with the splitting between different confined modes.

In this report, we present a full study of the polarization properties of the light emitted from co-existing 2D and 1D polariton condensates in a GaAs-based microcavity pumped in the conventional intraband OPO regime, as a function of the angle of the linear polarization of the excitation. Our experiments confirm the previously reported results for the 2D case, however, by reducing the dimensionality of the system from 2D to 1D, the polarization properties are strongly modified. By rotating the polarization plane of the pump beam, we observe an abrupt switching behavior of the OPO condensate emission between two highly linearly polarized states. Interestingly, the switching between these states occurs with the double frequency of that of the rotation of the pump's polarization plane. An extension of the existing spin-dependent semiclassical Boltzmann kinetic equations, taking explicitly into account the large polarization splitting value, is presented and fits excellently the experimental data. Real-space simulations done with Gross-Pitaevskii equations also confirm our interpretation of the experiments.

II. EXPERIMENTAL DETAILS

The sample[30] is based on a GaAs λ microcavity sandwiched between two 16 (20) pairs of AlAs/$Al_{0.15}Ga_{0.85}As$ distributed Bragg reflectors (DBR). A 10-nm-wide GaAs/$Al_{0.3}Ga_{0.7}As$ single quantum well is placed in the antinode of the confined optical field; its energy integrated emission under nonresonant excitation conditions is depicted in Fig. 1(a). Strong light-matter coupling results in the formation of upper and lower polariton branches with a Rabi splitting of $\hbar\Omega = 4.2$ meV at zero detuning. Further details of the system, with special emphasis on its coherence properties and the coexistence of 2D and 1D condensates, have been reported previously.[31] From the Fourier spectrum of the $g^{(1)}$ function, a lifetime of $\sim$2 ps has been determined. The sample is cooled down to a temperature of $T = 10$ K in a cold finger cryostat. It is excited with a continuous-wave, ring-cavity Ti:Al_2O_3 laser with a mono-mode linewidth of $\sim$75 kHz in an OPO configuration [see Fig. 1(b)]. The laser is focused onto a spot of $\sim$50 μm diameter. Figure 1(c) shows a scheme of the experimental setup. The overall numerical aperture of the optical system is 0.32, limited by the

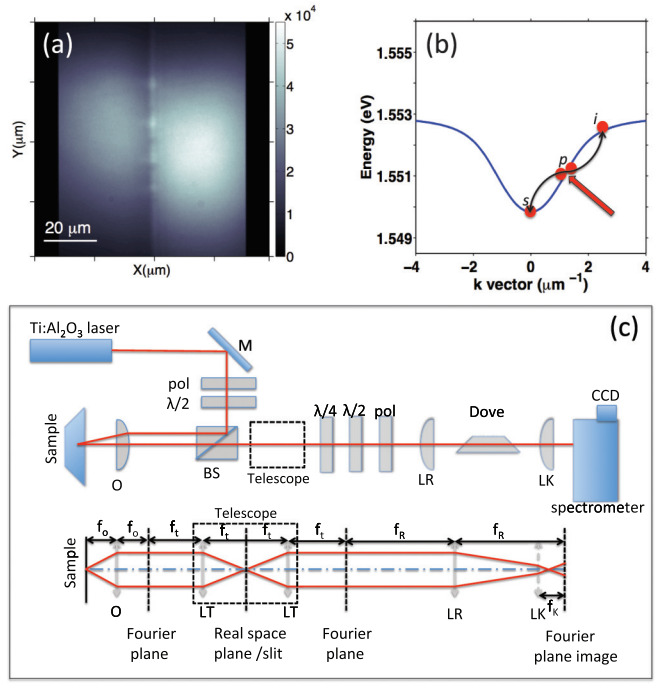

FIG. 1. (Color online) (a) Energy-integrated emission image of the sample for non-resonant excitation. (b) Scheme of the OPO excitation configuration:*p, s, i* correspond to the pump, signal and idler states, respectively. (c) Scheme of the experimental setup: The pump laser is passed via mirror "M" through polarization optics (linear polarizer "pol", half-wave plate "$\lambda/2$" and a beam-splitter "BS". It is focused onto the sample by an objective "O", which also collects the emission from the sample. This emission is passed through a telescope and polarization optics (quarter-wave plate "$\lambda/4$", etc.). The lenses "LR" and "LK" image the Fourier plane (momentum space) of the objective lens "O", while, if lens "LK" is removed, lens "LR" images the real space. The dove prism is used to rotate the image, when needed. The lower part shows the telescope in more detail: A slit is placed in the common focal plane of two lenses "LT" with focal length f_t. f_O, f_R and f_K are the focal lengths of the objective, "LR" and "LK" lenses, respectively.

components of the imaging optics, corresponding to a wave vector range of ± 2.5 μm^{-1} or collection angles of $\pm 20^\circ$. For momentum-space imaging, an additional lens (LK) is placed in the optical path in order to image the Fourier plane of the collection lens (O). The polarization is analyzed with a sequence of polarization optics consisting of a half-wave plate, quarter-wave plate, and linear polarizer.

III. RESULTS AND DISCUSSION

A. Real- and momentum-space imaging

1. 2D phase-matching conditions

For our experiments, we exploit the presence of otherwise undesired defects in the sample. Most semiconductor microcavities exhibit different kinds of defects due to strain relaxation during the growth process, which originates from impurities or lattice constant mismatch of the different semiconductor layers. The latter is a typical phenomenon of the multilayer DBR structure and leads to cross-hatching,[32] with

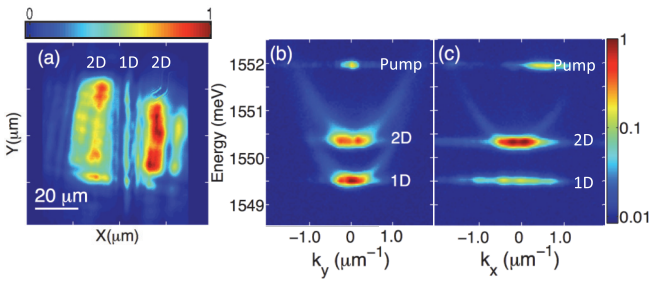

FIG. 2. (Color online) Real-space emission, and polariton dispersion for 2D phase-matching conditions. In (a), the normalized real-space emission is shown, integrated in energy and in a linear false-color scale, in a region of the sample where the planar cavity is split by a line defect; (b) shows the dispersion taken along the axis of the 1D system. Here, both systems show nonlinear emission from the bottom of their respective branch. In (c), the dispersion is normal to the 1D system: marked differences are seen, the 1D system shows no dispersion while the 2D remains the same. A logarithmic false-color scale is used for (b) and (c).

1D defects along the crystallographic axes and this is the plausible origin of the 1D defect we choose to investigate. Figure 1(a) shows the nonresonantly excited emission of the studied natural wire. We note that the luminescence is not arising from a defect but from a region of the sample where defects of the DBRs create localized states, similarly to what has been reported.[33,34] In Fig. 2(a), the real-space emission, integrated in energy, of an area around the defect is shown for excitation in the OPO configuration using the appropriate phase-matching conditions. The system is pumped ∼1.7 meV above the bottom of the 2D-LPB with an excitation energy of 1551.9 meV and an in-plane wave vector of $k_x \sim 2.0\ \mu\mathrm{m}^{-1}$, corresponding to a pump angle of 14.7°.

The angle (or, equivalently, the corresponding k value) of the excitation cannot be extracted from the momentum-space images [see Figs. 2(b) and 2(c)]. What is seen there is reflected plus scattered laser light. The component of the wave vector parallel to the wire is basically negligible. Furthermore, in order to keep the experimental realization of the OPO configuration as simple as possible, the experiments are restricted to the most symmetric situation, i.e., keeping the plane of incidence normal to the axis of the wire ($k_y = 0$). If the plane of incidence would not be normal to the axis wire, one would be changing the OPO configuration and simultaneously more complicated polarization selection rules would apply.

The emission in the area of the spot shows two rather rectangular shaped 2D condensates, with an 1D wire condensate vertically aligned in-between them. The particular rectangular shape and lines of the emission support the idea of strong cross-hatching due to DBR strain relaxation. The long-range coherence properties of this system have been studied and confirm the presence of a macroscopic quantum condensate.[31]

Figures 2(b) and 2(c) show the energy-momentum dispersion along the k_y and k_x directions, respectively. For the k-space imaging, we use a telescope, with a slit in the real-space plane [see Fig. 1(c)], in order to filter spatially the emission from the 2D area. The results shown in Fig. 2(b) have been obtained with the slit in the telescope set in such a way that the intensities of the 2D and 1D condensates are similar so that their dispersion characteristics can be compared simultaneously. In the k_y direction, parallel to the wire [Fig. 2(b)], two dispersions are clearly observed, an energetically lower and another higher one corresponding to the LPBs of the 1D and 2D systems, respectively. Strong emission located in momentum space at the bottom of the LPBs at $\boldsymbol{k} = 0$ indicates that phase-matching conditions are sufficiently fulfilled for both the 1D and 2D systems. For a pump power $P = 164$ mW, well above the threshold $P_{\mathrm{th}} = 76$ mW, two condensates are formed at the lowest subbands, $E^{1D} = 1549.5$ meV and $E^{2D} = 1550.2$ meV, respectively. Figure 2(c) shows the dispersion along the k_x direction, perpendicular to the wire. The additional confinement in this direction leads to a further quantization of the microcavity states[11,35] and in particular to a flat polariton dispersion in the direction normal to the wire at the lowest energy.

2. 1D phase-matching conditions

It is possible to selectively generate the 1D condensate only by fine adjustment of the excitation to the phase-matching conditions of the wire, i.e., lowering the excitation energy to $E = 1550.8$ meV and choosing an in-plane wave vector of $k_x \sim 1.55\ \mu\mathrm{m}^{-1}$, corresponding to a pump angle of 11.4°, as demonstrated in the real-space image in Fig. 3(a). Now, only the emission of the 1D wire is observed, while no condensation occurs in 2D. Figures 3(b) and 3(c) show the polariton dispersion parallel and perpendicular to the wire, respectively, and confirm the presence of a wire condensate at $\boldsymbol{k} = 0$ and the absence of the 2D condensate. Note that the excitation energy is still well above the 2D condensate energy, as observed in Fig. 2, and also above the LPB, but the strict 2D phase-matching conditions impede the formation of the 2D OPO.

One should note that the main purpose of the momentum-space images, shown in the Figs. 2(b), 2(c), 3(b), and 3(c) is to visualize the dispersion relations of the 1D and 2D system

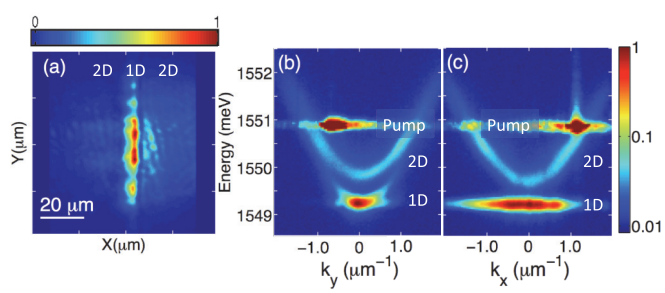

FIG. 3. (Color online) Real-space emission, and polariton dispersion for 1D phase-matching conditions. In (a), the normalized real-space emission, integrated in energy, at the same region as in Fig. 2 is shown in a linear false-color scale, but now there is only significant emission from the 1D condensate. (b) Dispersion taken along the axis of the 1D system. Here, the 2D polariton dispersion does not show condensation, whereas in the 1D system nonlinear emission is found. In (c), the dispersion is normal to the 1D system: marked difference are seen, the 1D system shows no dispersion while the 2D remains the same. A logarithmic false-color scale is used for (b) and (c).

for different directions. A quantitative analysis of the results shown in these figures is neither needed nor performed for our studies. Slightly different alignment of the imaging optics produces differences between Figs. 2(b) and 2(c) regarding intensities, energy shifts and dispersion curvatures. The same effect is observed comparing Figs. 3(b) and 3(c).

The larger energy blue shifts seen in Figs. 2(b) and 2(c) as compared to those in Figs. 3(b) and 3(c) arise from differences in the occupancy of the different states. The higher density of 2D polaritons, and consequently the increased polariton-polariton interactions in the condensed phase [see Figs. 2(b) and 2(c)], leads to a blue shift of ~0.5 meV for the 2D system with respect to the noncondensed situation [see Figs. 3(b) and 3(c)]. For the same reason, the condensed 1D polariton state shifts also to higher energies, although by a smaller amount.

B. Polarization studies

We now investigate in detail the polarization properties of the system. The polarized emission of the signal state is studied, as a function of the angle, θ_P, of the linear polarization of the pump laser, for phase-matching conditions set for the 2D LPB. Spatially resolved false-color maps of the degree of linear polarization (DLP) of the emission are shown in Fig. 4. The DLP $= (I_\perp - I_\parallel)/(I_\perp + I_\parallel)$ is obtained for each point from spatial emission patterns, similar to those shown in Figs. 2(a) or 3(a) but polarization-resolved ones. The orientation, θ_P, of the linearly polarized excitation varies for the four panels: $\theta_P = 0$ (normal to the wire), $\theta_P = 20°$, $\theta_P = 45°$ (diagonal) and $\theta_P = 90°$ (parallel to the wire). In Fig. 4(a), the pump polarization is aligned perpendicularly to the wire and it is observed that the polarization of the 2D polaritonic emission is rotated by 90° with respect to that of the pump laser (blue colors). However, the polarization of the light emitted from the wire coincides with that of the pump polarization (red colors). In Fig. 4(b), for $\theta_P = 20°$, the 2D emission shows a slight decrease in the DLP, while the DLP of the 1D system becomes nearly zero. Figure 4(c) corresponds to the diagonally polarized excitation: now the DLP of the 2D emission vanishes, whereas in the 1D system, a high negative DLP is observed. Finally, when the system is excited with polarization parallel to the wire [see Fig. 4(d), $\theta_P = 90°$], both polarizations of the 1D and 2D emissions are rotated by 90° with respect to that of the pump laser.

Looking into the details of the DLP patterns shown in Fig. 4, a fine structure is observed, which is not further studied here since we are interested in the overall DLP behavior as a function of the laser polarization plane. However, the resolution of this fine structure demonstrates the power of polarization-resolved emission studies compared to regular photoluminescence ones [see Figs. 1(a), 2(a), and 3(a), where this fine structure is not resolved].

Figure 5 compiles the emission DLP as a function of θ_P in more detail. These data are obtained by integration and normalization of areas in the DLP maps that are depicted as dashed boxes in Fig. 4. Figures 5(a) and 5(b) show the results discussed above for 2D phase-matching conditions, while Fig. 5(c) corresponds to 1D phase-matching conditions.

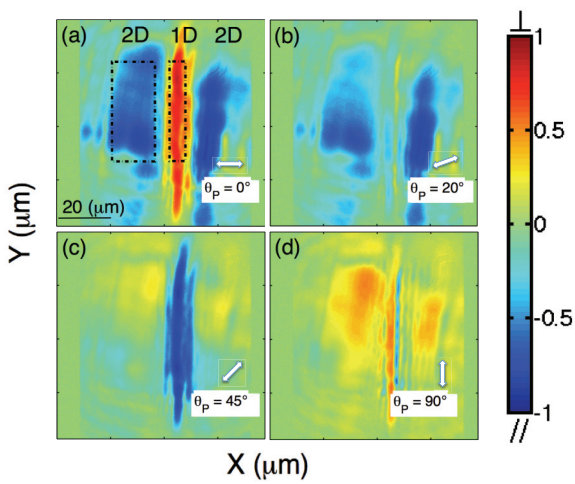

FIG. 4. (Color online) False-color intensity maps of the DLP for selected values of θ_P. The arrows depict the plane of the pump's polarization. In (a), $\theta_P = 0°$, the polarization of the emission from the 2D system is opposite to that of the laser, while the 1D condensate keeps the same polarization of the pump. In (b), $\theta_P = 20°$, the DPL of the 2D condensate decreases and that of the 1D system vanishes. In (c), $\theta_P = 45°$, the 2D condensate exhibits a negligible DLP, while the 1D emission is highly polarized parallel to the wire. In (c), $\theta_P = 90°$, both condensates show an inversion of the polarization plane with respect to that of the laser. Dashed boxes show the area of integration, used to obtain the curves in Fig. 5.

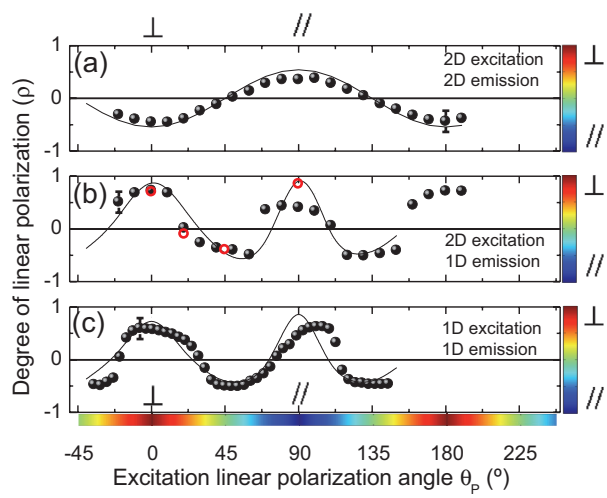

FIG. 5. (Color online) Degree of linear polarization as a function of the linear polarization angle of the pump: Color bars next to the vertical and bottom axis represent the DLP of the emission and the pump, respectively. At $\theta_P = 0°$ ($\theta_P = 90°$), the laser is polarized normal (parallel) to the wire, as indicated by the ⊥ (‖) symbol. The symbols at the ordinates indicate the main orientation of the emission's polarization plane: ⊥ (‖) perpendicular (normal) to the wire axis. (a) The evolution of the DLP for the 2D system, for 2D phase-matching conditions. (b) The evolution of the DLP for the 1D system, for 2D phase-matching conditions. (c) The evolution of the DLP for the 1D system, for 1D phase-matching conditions. The solid lines (red open points) are calculated DLPs using the Boltzmann (GP) model.

1. Analysis of the 2D case

For the 2D condensate, Fig. 5(a), it is observed that the DLP changes, in a sinusoidal-like fashion, between −0.5 and 0.4, when varying the pump polarization angle θ_P. In particular, for perpendicular (⊥) and parallel (∥) polarized excitation with respect to the wire, the emission polarization is rotated by 90°. Linear polarization inversion is a typical behavior of microcavity polariton systems, which has been previously observed experimentally[27] and explained theoretically[19] in terms of polariton-polariton scattering. It confirms that in our system the interaction constants of same- and opposite-spin polaritons are of opposite signs and that the interaction between polaritons of opposite spins is attractive.[36] We note that when the OPO is pumped with circular polarization, the signal state is completely driven by the laser, as in Ref. 17, and inversion is neither observed for the 2D nor the 1D condensate.

2. Analysis of the 1D case

The DLP of the 1D wire emission for the 2D phase-matching conditions, Fig. 5(b), is remarkably different to the one observed for the 2D condensate. Now the emission is polarized either parallel or normal to the wire with high DLP up to −0.7 and 0.8, respectively. Moreover, the transition between these two polarization states is very abrupt. Note that the diagonal and circular polarization components (not shown) for any angle of polarization of the excitation remain below 15% and 10%, respectively. Linear polarization inversion has also been observed in interband parametric scattering processes in polariton wires[13,29] for specific excitation conditions. Furthermore, our study, performed over the full range of the angles of the pump's polarization, reveals not only the inversion but also switching of the polarization with the double frequency of the rotation of the pump's polarization plane. Figure 5(c) shows the evolution of the wire DLP for 1D-condensate phase-matching conditions: compared with Fig. 5(b) no significat differences are observed, suggesting that the 2D and 1D systems are decoupled.

C. Theoretical modeling

In order to describe and interpret our experimental results, we have used two complementary models: (i) the coupled 2D spinor Gross-Pitaevskii equation for excitons and Schrödinger equation for photons;[37] (ii) the semiclassical Boltzmann equations for populations and pseudospins of pump, signal and idler.[38] The former model allows to obtain spatial images similar to the experimental ones (see Fig. 4), but is numerically very heavy, while the latter one captures the essence of the physics involved and allows to reproduce the DLP in the 2D and 1D cases (see Fig. 5) when there is no need for spatial resolution.

1. Gross-Pitaevskii approach

In the first model, we write the coupled equations for a 2D four-component exciton-photon wave-function composed of a photonic fraction $\psi_{\uparrow\downarrow}(x,y)$ and an excitonic fraction $\varphi_{\uparrow\downarrow}(x,y)$:

$$i\hbar\frac{\partial\psi_{\uparrow\downarrow}}{\partial t} = -\frac{\hbar^2}{2m_{\rm ph}}\Delta\psi_{\uparrow\downarrow} + \frac{\hbar\Omega_R}{2}\varphi_{\uparrow\downarrow} + H_x\psi_{\downarrow\uparrow} + U\psi_{\uparrow\downarrow} - \frac{i\hbar}{2\tau_{\rm ph}}\psi_{\uparrow\downarrow} + P_{\uparrow\downarrow} + f_{\uparrow\downarrow}, \quad (1)$$

$$i\hbar\frac{\partial\varphi_{\uparrow\downarrow}}{\partial t} = -\frac{\hbar^2}{2m_X}\Delta\varphi_{\uparrow\downarrow} + \frac{\hbar\Omega_R}{2}\psi_{\uparrow\downarrow} + \alpha_1|\varphi_{\uparrow\downarrow}|^2\varphi_{\uparrow\downarrow} + \alpha_2|\varphi_{\downarrow\uparrow}|^2\varphi_{\uparrow\downarrow}. \quad (2)$$

Here, $m_{\rm ph} = 4\times10^{-5}\,m_0$ is the photon mass, $m_X = 0.6\,m_0$ is the exciton mass, m_0 is the free electron mass, $\hbar\Omega_R = 4.2$ meV is the Rabi splitting, $\alpha_1 = 6\,E_b\,a_B^2$ and $\alpha_2 \sim -0.01\,\alpha_1$ are the triplet and singlet interaction constants,[36] respectively. $E_b = 10$ meV is the exciton binding energy and $a_B = 10$ nm is the exciton Bohr radius. The potential acting on photons, confining them in the trap of width 4.25 μm and depth 0.6 meV, is described by U. $\tau_{\rm ph} = 1$ ps is the photon lifetime (the exciton decay is neglected), P is the quasiresonant pumping term, exciting the system at a given frequency $\omega \approx 1.6$ meV$/\hbar$ above the bottom of the polariton branch and f is the noise, which serves to account for the effects of spontaneous scattering. Pumping provides an average of 10 particles in a 0.25-μm-wide unit cell in the steady state, and the spontaneous scattering creates 0.01 particles. The term $H_x = 30\,\mu$eV describes the effective magnetic field (polarization splitting of 60 μeV) acting only inside the 1D wire.

The results of the simulations performed for the same four orientations of the pump polarization as in the experiments ($\theta_P = 0°$,20°,45°, and 90°) are presented in Fig. 6, which reproduce qualitatively the experimental observations of Fig. 4. In these simulations, as in the experiments, in the 2D region, the polarization is always inverted because of the opposite signs of α_1 and α_2, while in the quantized 1D region the polarization is determined by an interplay between the signs of the α's coefficients and the splitting between the parallel and transverse polarized modes, as explained in detail below.

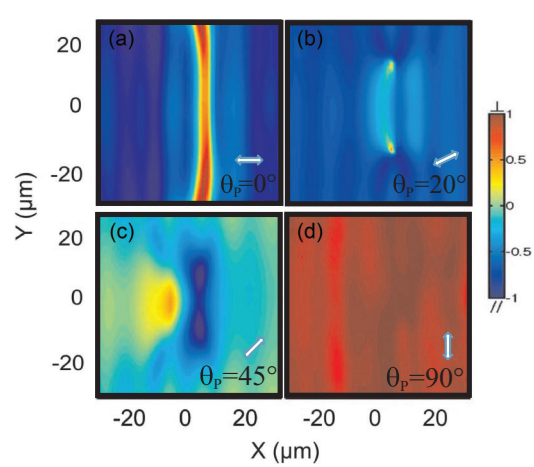

FIG. 6. (Color online) Calculated false-color intensity maps of the DLP of the signal state for selected values of θ_P: (a) 0°, (b) 20°, (c) 45°, and (d) 90°.

Note that in the simulations, the 2D condensate extends over the entire area shown in the figure, in contrast to the experiments, where the condensate's extension is about 40 μm. Also, the DLP is higher in the calculations than in the experiments, however, a qualitative overall agreement between experiment and theory is evident. Although this model is nicely fitting the experiments, it is quite demanding numerically because of the need for a large 2D grid, a small step size to describe accurately the potential defect and the profiles of the modes, and long calculation times necessary to obtain spontaneous OPO with a relatively weak noise.

2. *Semiclassical Boltzmann approach*

This approach considers only the three strongest populated modes (pump, signal and idler), while all others are neglected, which greatly improves the computational efficiency of the model. Using the experimental evidence of decoupled 2D and 1D systems, we calculate these regimes separately. The system of equations describing the dynamics of the pump, signal and idler populations and their pseudospins is written as

$$\frac{dN_{k\uparrow,\downarrow}}{dt} = -\frac{N_{k\uparrow,\downarrow}}{\tau_k} + \left(\frac{dN_{k\uparrow,\downarrow}}{dt}\right)\bigg|_{\text{rot}} + \left(\frac{dN_{k\uparrow,\downarrow}}{dt}\right)\bigg|_{p-p} + P_k, \tag{3}$$

$$\frac{d\mathbf{S}_k}{dt} = -\frac{\mathbf{S}_k}{\tau_k} + \left(\frac{d\mathbf{S}_k}{dt}\right)\bigg|_{\text{rot}} + \left(\frac{d\mathbf{S}_k}{dt}\right)\bigg|_{p-p} + \mathbf{P}_k, \tag{4}$$

where $N_{k\uparrow,\downarrow}$ are the z projections of the populations and $\mathbf{S}_k$ is the in-plane pseudospin. Thus $\mathbf{S}_k$ contains the S_x and S_y components, while the S_z projection is given by $N_\uparrow - N_\downarrow$. Here, $k = p,s,i$ corresponds to the pump, signal and idler states. τ_k is the lifetime of the corresponding state, and P_k is the pumping term ($P_p = P$, $P_{s,i} = 0$). The semiclassical equations take into account the spontaneous and the stimulating scattering processes. We solve these equations separately for each case presented in Fig. 5: 2D [see Fig. 5(a)], 1D out-of-resonance [see Fig. 5(b)], and 1D resonant case [see Fig. 5(c)]. All other relevant details of the model are given in the Appendix.

These equations were used very efficiently to describe the polarization dynamics in various OPO configurations,[27,39] but always in the 2D case of planar cavities. The result of the simulation for the 2D system is presented as a solid line in Fig. 5(a) giving a very good agreement with the experimental data and showing polarization inversion.

However, the observed effects in the 1D case are not limited to a simple polarization inversion, and the model requires to be extended. The strong splitting between the linearly polarized polariton modes has not been treated so far. This splitting is of the order of 0.1 meV, and its effect is not limited to a simple precession of the polariton pseudospin in an effective magnetic field, analogous to the TE-TM field. It also affects energy conservation of polariton-polariton inelastic scattering processes, causing slightly different scattering rates

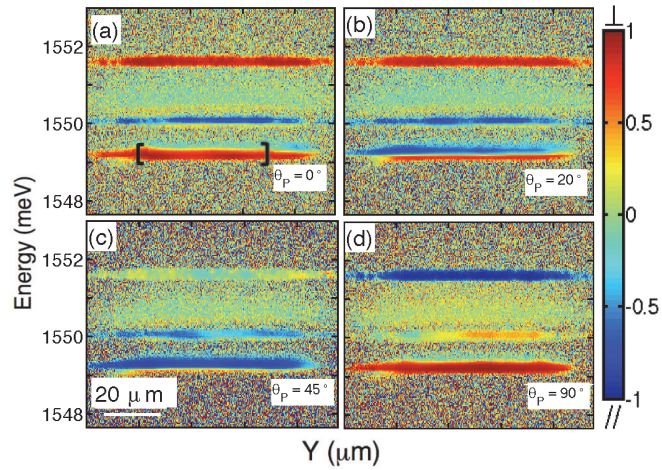

FIG. 7. (Color online) Spectrally resolved false-color polarization maps for the degree of linear polarization, with the same selected values of θ_P as in previous figures. In (a), the 1D system shows emission polarized normal to the wire at ∼1549 meV. (b) Two lines with opposite polarization in the 1D condensate are resolved: at low (high) energy, the emission is polarized normal (parallel) to the wire. In (c), again a single line is emitting. (d) The emission from the 1D system becomes again polarized normal to the wire. The square brackets in (a) delimit the range, along the wire, used to integrate the polarized emission that is shown in Fig. 8.

into parallel and normal modes. This can be taken into account in the three-level model by introducing a new term to Eq. (4) describing the pseudospin dynamics of signal and idler:

$$+\mathbf{e}_x \delta W \left(\frac{dN_j}{dt}\right)\bigg|_{p-p}, \tag{5}$$

where $j = s,i$ stands for signal and idler, respectively. This term describes the dynamics of pseudospin projection on the unit vector $\mathbf{e}_x$ along the x axis of polaritons scattered into s and i and is proportional to the relative difference between the scattering amplitudes into the linear modes $\delta W = (W_\perp - W_\parallel)/(W_\perp + W_\parallel)$. δW originates from the difference in the overlap integrals between the states localized in the trap and the extended propagating states of the pump and the idler. Indeed, the trap is wide enough to contain several quantized levels. The highest levels of the two orthogonal polarizations that become strongly populated in the experiments (see Figs. 7 and 8) do not have the same transverse quantum number n. Otherwise, the transverse-polarized state $\perp$ would be higher in energy than the longitudinal-polarized state $\parallel$ because of the longitudinal-transverse splitting. The overlap integrals, contained in the scattering rates W, exhibit a $1/n$ dependence, implying that scattering into the lower lying states is favored. On the other hand, phase matching conditions favor the population of higher lying ones. This balance leads actually to a further decrease of δW. Thus this term is comparable to the one responsible for polarization inversion (the latter is proportional to α_2/α_1) and the competition between them can determine the relative sign of the signal's and pump's DLP. Values of $\alpha_2/\alpha_1 = -0.01$ and $\delta W = 0.008$ are typically used in the simulations.

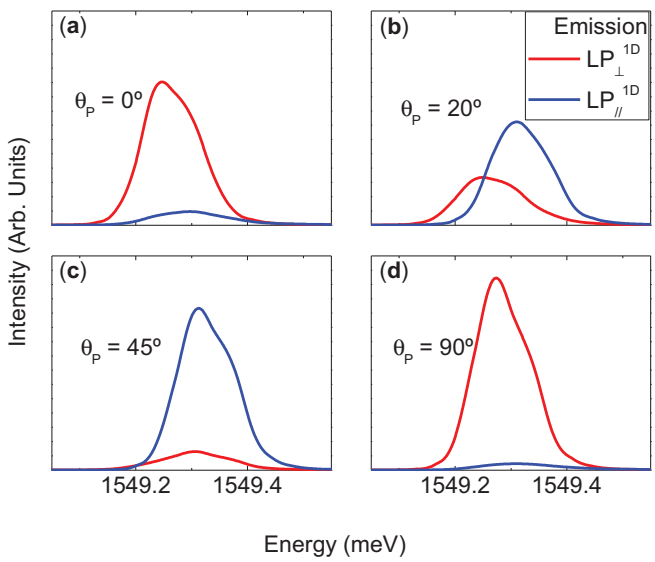

FIG. 8. (Color online) Emission spectra of the wire condensate for different θ_P. Polarization fine structure is observed and attributed to internal strain. The modes $LP_{\parallel}^{1D}$ and $LP_{\perp}^{1D}$ are polarized parallel and normal to the wire, respectively.

This additional contribution would produce a linear polarization in the signal even for an unpolarized pump. Since scattering into one of the two polarization eigenstates is more efficient, it becomes populated stronger, which leads to an increase of the DLP. The interplay between the polarization inversion and the generation of linear polarization explains the observed DLP of the signal state in Figs. 5(b) and 5(c) for 2D and 1D phase matching conditions, respectively. Since the linear polarization is generated by the presence of the confining potential, the resulting behavior is essentially the same for both cases.

A good agreement between both models concerning the DLP of the wire is obtained: the results of the GP simulation of Fig. 6 are depicted as red open points in Fig. 5(b). They coincide well with the results of the Boltzmann model. Both theoretical approaches allow us to conclude that the peculiar behavior of the DLP for the 1D case is a result of the competition between the polarization inversion mechanism and the difference between the scattering rates towards the polarization eigenstates, which are quantized in the wire. The inversion mechanism is based on the spin-anisotropy of the interactions, which acts both for 2D and 1D. The nonlinearity of the OPO configuration does not allow representing the signal DLP simply as the sum of the two effects and the resulting curve becomes not sinusoidal. This competition and the nonlinearities imply that the results would differ for a wire characterized by different parameters.

D. Polarization fine structure

The Boltzmann model renders well the change of the DLP for the 1D and 2D condensates and implies orthogonal, linearly polarized states with different polariton-polariton scattering rates. Indeed, our experiments reveal the existence of such polarization fine structure. We show in Fig. 7 spectrally and spatially resolved polarization false-color intensity maps of the 1D system for varying angle θ_P of the polarization of the pump under 2D phase-matching conditions. In the x direction, $\sim$1 μm has been integrated to obtain these maps. Red and blue represent, as in the previous figures, linear polarizations normal and parallel to the wire axis, respectively. Note that higher values for the DLP than those depicted in Figs. 4 and 5 are obtained, since the nonpolarized emission arising from the uncondensed phase is now spectrally filtered out.

The two energetically highest lying lines at $\sim$1552 meV and $\sim$1550 meV correspond to the excitation laser and the emission from the 2D system, respectively. In Fig. 7(a), the angle θ_P is zero and the polarization of the emission at $\sim$1549 meV of the 1D system is the same as that of the excitation. However, for $\theta_P = 20^\circ$, shown in Fig. 7(b), the emission of the 1D system consists of two split lines, each one with opposite linear polarization. In Fig. 7(c), $\theta_P = 45^\circ$ and the 1D system again shows just a single emission line polarized parallel to the wire. For an angle $\theta_P = 90^\circ$, the 1D system exhibits again emission of high DLP and polarization inversion occurs.

The polarized wire emission integrated along the wire, in the range enclosed by square brackets in Fig. 7, is shown in more detail in Fig. 8 for selected polarizations of the pump. The emission spectra exhibit shoulders, which suggests that more than one mode are excited, however, in the presented measurements they cannot be resolved due to experimental limitations. Furthermore, for all pump polarizations, a polarization splitting of the wire LPB into two orthogonal linearly polarized modes $LP_{\parallel}^{1D}$ and $LP_{\perp}^{1D}$ is obtained: they are polarized parallel and normal to the wire, respectively. Large polarization splitting in polariton wires has been observed previously and attributed to external strain.[13,29,35] In our samples, we observe marked cross-hatching suggesting the presence of large internal strain fields, which are possibly the source of the polarization splitting.[32] In Fig. 8, the splitting between the linearly polarized modes appears to be different in each of the Figs. 8(a)–8(d). One must consider that several components are present in each emission band (not resolvable due to experimental limitations) and that the relative changes of intensity of each component, together with the blue shifts due to polariton-polariton interactions, lead to an apparent change of the splitting. In Figs. 8(a) and 8(d), the pump is polarized normal and parallel to the wire, respectively: in both cases, the dominant emission originates from the energetically lower lying, polarized normal to the wire, mode $LP_{\perp}^{1D}$, while the intensity of parallel polarized mode $LP_{\parallel}^{1D}$ is small, giving rise to a high DLP. The spectra in Fig. 8(b) ($\theta_P = 20^\circ$) exhibit closer emission intensities from both lines, and therefore a vanishing DLP is observed in Figs. 4 and 5. Finally, in Fig. 8(c), the pump's polarization is diagonal and the emission arises mainly from the parallel polarized mode $LP_{\parallel}^{1D}$ rendering again a high DLP. In both cases shown in Figs. 8(b) and 8(c), the larger emission arises from the energetically higher lying state, $LP_{\parallel}^{1D}$, in contrast to what would be expected for a thermal distribution. However, polariton condensates, especially in the OPO regime, are highly nonthermal. This is similar to the observation in Ref. 40,

where a splitting in the linear polarization is reported and a larger occupancy of the higher lying state is observed. This fact has been attributed to crystallographic anisotropy and pinning.

IV. CONCLUSIONS

In summary, we have investigated polarization properties of 2D and 1D polariton condensates as a function of angle of the pump's polarization plane, θ_P. In both cases, we observe polarization inversion for a pump polarization parallel to the wire. However, for the 1D wire, as the polarization plane of the excitation is rotated, we observe a switching between two states of high DLP. The switching between the two states occurs with the double frequency of the rotation of the pump's polarization plane. Two models, based on semiclassical Boltzmann kinetic equations and the Gross-Pitaevskii equation, respectively, are presented and reproduce well the polarization rotation for the 2D condensate and in particular the halved periodicity of the rotation for the 1D limit.

ACKNOWLEDGMENTS

This work was supported by grants FP7 ITNs Clermont4 (235114), Spin-optronics (237252) and INDEX (289968), the Spanish MEC (MAT2011-22997), and CAM (S-2009/ESP-1503).

APPENDIX

Here, we give the details of the semiclassical Boltzmann approach used to simulate the DLP in the 2D and 1D cases. The rotational terms in Eqs. (3) and (4) describe the action of various effective magnetic fields associated with polarization splittings:

$$\left(\frac{dN_{k\uparrow}}{dt}\right)\bigg|_{\text{rot}} = -\left(\frac{dN_{k\downarrow}}{dt}\right)\bigg|_{\text{rot}} = \mathbf{e}_z \cdot [\mathbf{S}_k \times \mathbf{\Omega}_{\text{LT},k}]\,, \tag{A1}$$

$$\left(\frac{d\mathbf{S}_k}{dt}\right)\bigg|_{\text{rot}} = [\mathbf{S}_k \times \mathbf{\Omega}_{\text{int},k}] + \frac{N_{k\uparrow} - N_{k\downarrow}}{2}\mathbf{\Omega}_{\text{LT},k}\,. \tag{A2}$$

$\mathbf{\Omega}_{\text{LT},k}$ is the effective magnetic field induced by the polariton TE-TM splitting,[28] $\mathbf{\Omega}_{\text{int}}$ is an effective field due to spin-anisotropic interactions:

$$\hbar\mathbf{\Omega}_{\text{int},\mathbf{k}} = 2\mathbf{e}_z \sum_{\mathbf{k}'} \left(V^{(1)}_{\mathbf{k},\mathbf{k}',0} - V^{(2)}_{\mathbf{k},\mathbf{k}',0}\right)(N_{\mathbf{k}'\uparrow} - N_{\mathbf{k}'\downarrow})\,, \tag{A3}$$

where $V^{(1)}$and $V^{(2)}$ are the matrix elements of polariton-polariton interactions described in detail below, and $\mathbf{e}_z$ is a unit vector in the z direction of the Stokes space, corresponding to circularly polarized light. Finally, the polariton-polariton scattering terms can be expressed as

$$\begin{aligned}\left(\frac{dN_{k\uparrow}}{dt}\right)\bigg|_{p-p} = \sum_{k',k''}\Big\{ & W^{(1)}_{k,k',k''}[(N_{k\uparrow} + N_{k'\uparrow} + 1)N_{k+k''\uparrow}N_{k'-k''\uparrow} - (N_{k+k''\uparrow} + N_{k'-k''\uparrow} + 1)N_{k\uparrow}N_{k'\uparrow}] \\ & + W^{(1)}_{k,k',k''}[(N_{k\uparrow} + N_{k'\downarrow} + 1)(N_{k+k''\uparrow}N_{k'-k''\downarrow} + N_{k+k''\downarrow}N_{k'-k''\uparrow}) + 2\mathbf{S}_{k+k''} \cdot \mathbf{S}_{k'-k''}] \\ & - [N_{k\uparrow}N_{k'\downarrow} + (\mathbf{S}_k \cdot \mathbf{S}_{k'})](N_{k+k''\uparrow} + N_{k'-k''\downarrow} + N_{k+k''\downarrow} + N_{k'-k''\uparrow} + 2) \\ & + 2W^{(12)}_{k,k',k''}[N_{k''\uparrow}(\mathbf{S}_{k'} \cdot \mathbf{S}_{k'-k''}) + N_{k'-k''\uparrow}(\mathbf{S}_{k'} \cdot \mathbf{S}_{k+k''}) - N_{k\uparrow}\mathbf{S}_{k'} \cdot (\mathbf{S}_{k'-k''} + \mathbf{S}_{k+k''})] \\ & + W^{(12)}_{k,k',k''}[(\mathbf{S}_k \cdot \mathbf{S}_{k+k''})(N_{k'-k''\uparrow} + N_{k'-k''\downarrow} - N_{k'\uparrow} - N_{k'\downarrow}) \\ & + (\mathbf{S}_k \cdot \mathbf{S}_{k'-k''})(N_{k+k''\uparrow} + N_{k+k''\downarrow} - N_{k'\uparrow} - N_{k'\downarrow})]\Big\},\end{aligned} \tag{A4}$$

$$\begin{aligned}\left(\frac{d\mathbf{S}_{\mathbf{k}}}{dt}\right)\bigg|_{p-p} = \sum_{\mathbf{k}',\mathbf{q}}\Bigg(& \frac{W^{(1)}_{\mathbf{k},\mathbf{k}',\mathbf{q}}}{2}\mathbf{S}_{\mathbf{k}}[N_{\mathbf{k}+\mathbf{q}\uparrow}N_{\mathbf{k}'-\mathbf{q}\uparrow} + N_{\mathbf{k}+\mathbf{q}\downarrow}N_{\mathbf{k}'-\mathbf{q}\downarrow} - N_{\mathbf{k}'\uparrow}(N_{\mathbf{k}+\mathbf{q}\uparrow} + N_{\mathbf{k}'-\mathbf{q}\uparrow} + 1) - N_{\mathbf{k}'\downarrow}(N_{\mathbf{k}+\mathbf{q}\downarrow} + N_{\mathbf{k}'-\mathbf{q}\downarrow} + 1)] \\ & + W^{(1)}_{\mathbf{k},\mathbf{k}',\mathbf{q}}[(\mathbf{S}_{\mathbf{k}+\mathbf{q}}(\mathbf{S}_{\mathbf{k}'} \cdot \mathbf{S}_{\mathbf{k}'-\mathbf{q}}) + \mathbf{S}_{\mathbf{k}'-\mathbf{q}}(\mathbf{S}_{\mathbf{k}'} \cdot \mathbf{S}_{\mathbf{k}+\mathbf{q}}) - \mathbf{S}_{\mathbf{k}'}(\mathbf{S}_{\mathbf{k}+\mathbf{q}} \cdot \mathbf{S}_{\mathbf{k}'-\mathbf{q}})] \\ & + \frac{W^{(2)}_{\mathbf{k},\mathbf{k}',\mathbf{q}}}{2}\{2(\mathbf{S}_{\mathbf{k}} + \mathbf{S}_{\mathbf{k}'})[N_{\mathbf{k}+\mathbf{q}\uparrow}N_{\mathbf{k}'-\mathbf{q}\downarrow} + N_{\mathbf{k}+\mathbf{q}\downarrow}N_{\mathbf{k}'-\mathbf{q}\uparrow} + 2(\mathbf{S}_{\mathbf{k}+\mathbf{q}} \cdot \mathbf{S}_{\mathbf{k}'-\mathbf{q}})] \\ & - [\mathbf{S}_{\mathbf{k}}(N_{\mathbf{k}'\uparrow} + N_{\mathbf{k}'\downarrow}) + \mathbf{S}_1(N_{\mathbf{k}\uparrow} + N_{\mathbf{k}\downarrow})](N_{\mathbf{k}+\mathbf{q}\uparrow} + N_{\mathbf{k}'-\mathbf{q}\uparrow} + N_{\mathbf{k}+\mathbf{q}\downarrow} + N_{\mathbf{k}'-\mathbf{q}\downarrow} + 2)\} \\ & - 2W^{(12)}_{\mathbf{k},\mathbf{k}',\mathbf{q}}\mathbf{S}_{\mathbf{k}}[(\mathbf{S}_{\mathbf{k}'} \cdot \mathbf{S}_{\mathbf{k}+\mathbf{q}}) + (\mathbf{S}_{\mathbf{k}'} \cdot \mathbf{S}_{\mathbf{k}'-\mathbf{q}})] \\ & + \frac{W^{(12)}_{\mathbf{k},\mathbf{k}',\mathbf{q}}}{2}\mathbf{S}_{\mathbf{k}'-\mathbf{q}}\{2[(N_{\mathbf{k}'\uparrow} + 1)N_{\mathbf{k}+\mathbf{q}\uparrow} + (N_{\mathbf{k}'\downarrow} + 1)N_{\mathbf{k}+\mathbf{q}\downarrow}] + (N_{\mathbf{k}+\mathbf{q}\uparrow} + N_{\mathbf{k}+\mathbf{q}\downarrow} - N_{\mathbf{k}'\uparrow} - N_{\mathbf{k}'\downarrow})(N_{\mathbf{k}\uparrow} + N_{\mathbf{k}\downarrow})\} \\ & + \frac{W^{(12)}_{\mathbf{k},\mathbf{k}',\mathbf{q}}}{2}\mathbf{S}_{\mathbf{k}+\mathbf{q}}\{2[(N_{\mathbf{k}'\uparrow} + 1)N_{\mathbf{k}'-\mathbf{q}\uparrow} + (N_{\mathbf{k}'\downarrow} + 1)N_{\mathbf{k}'-\mathbf{q}\downarrow}] + (N_{\mathbf{k}'-\mathbf{q}\uparrow} + N_{\mathbf{k}'-\mathbf{q}\downarrow} - N_{\mathbf{k}'\uparrow} - N_{\mathbf{k}'\downarrow})(N_{\mathbf{k}\uparrow} + N_{\mathbf{k}\downarrow})\}\Bigg).\end{aligned} \tag{A5}$$

An analogue expression to Eq. (A4) holds for $\left(dN_{k\downarrow}/dt\right)\big|_{p-p}$. These equations have been developed in the past and used to describe numerous experiments on the polariton OPO.[27,39] They are presented here for the reader's convenience. The terms $W^{(1)}$, $W^{(2)}$, and $W^{(12)}$ represent polariton-polariton interactions in different spin configurations:

$$W^{(1)}_{k,k',k''} = \frac{2\pi}{h}\left|V^{(1)}_{k,k',k''}\right|^2\delta(\Omega_k + \Omega_{k'} - \Omega_{k+k''} - \Omega_{k-k''}), \quad \text{(A6)}$$

$$W^{(2)}_{k,k',k''} = \frac{2\pi}{h}\left|V^{(2)}_{k,k',k''}\right|^2\delta(\Omega_k + \Omega_{k'} - \Omega_{k+k''} - \Omega_{k-k''}), \quad \text{(A7)}$$

$$W^{(12)}_{k,k',k''} = \frac{2\pi}{h}\mathrm{Re}\left(V^{(1)}_{k,k',k''}V^{*(2)}_{k,k',k''}\right) \times \delta(\Omega_k + \Omega_{k'} - \Omega_{k+k''} - \Omega_{k-k''}). \quad \text{(A8)}$$

Equations (A6)–(A8) are written for the most general case. Taking into account the excitonic fraction of the relevant states, and assuming a contact interaction for the matrix elements V, therefore not depending on k, $V^{(1)}$ and $V^{(2)}$ correspond to the α_1 and α_2 parameters of the Gross-Pitaevskii Eq. (2). We assume for the calculations the usual ratio $\alpha_2/\alpha_1 \sim -0.01$ (see Refs. 27 and 36), which obtains a negative $W^{(12)}_{0,k_p,k_p}$. Since the expression for the in-plane pseudospin reduces to

$$\frac{d\mathbf{S}_s}{dt} = W^{(12)}_{0,k_p,k_p}(N_{\uparrow p} + N_{p\downarrow})\mathbf{S}_p\ , \quad \text{(A9)}$$

the negative sign of $W^{(12)}_{0,k_p,k_p}$ leads to polarization inversion during spontaneous scattering from the pump to the signal state.

*jorge.cuadra@uam.es

[1] C. Weisbuch, M. Nishioka, A. Ishikawa, and Y. Arakawa, Phys. Rev. Lett. **69**, 3314 (1992).

[2] J. Kasprzak, M. Richard, S. Kundermann, A. Baas, P. Jeambrun, J. M. J. Keeling, F. M. Marchetti, M. H. Szymanska, R. Andre, J. L. Staehli, V. Savona, P. B. Littlewood, B. Deveaud, and L. S. Dang, Nature (London) **443**, 409 (2006).

[3] K. G. Lagoudakis, M. Wouters, M. Richard, A. Baas, I. Carusotto, R. Andre, L. S. Dang, and B. Deveaud-Pledran, Nat. Phys. **4**, 706 (2008).

[4] D. Sanvitto, F. M. Marchetti, M. H. Szymanska, G. Tosi, M. Baudisch, F. P. Laussy, D. N. Krizhanovskii, M. S. Skolnick, L. Marrucci, A. Lemaitre, J. Bloch, C. Tejedor, and L. Vina, Nat. Phys. **6**, 527 (2010).

[5] A. Amo, D. Sanvitto, F. P. Laussy, D. Ballarini, E. del Valle, M. D. Martin, A. Lemaitre, J. Bloch, D. N. Krizhanovskii, M. S. Skolnick, C. Tejedor, and L. Vina, Nature (London) **457**, 291 (2009).

[6] A. Amo, S. Pigeon, D. Sanvitto, V. G. Sala, R. Hivet, I. Carusotto, F. Pisanello, G. Leménager, R. Houdré, E. Giacobino, C. Ciuti, and A. Bramati, Science **332**, 1167 (2011).

[7] M. Sich, D. N. Krizhanovskii, M. S. Skolnick, A. V. Gorbach, R. Hartley, D. V. Skryabin, E. A. Cerda-Mendez, K. Biermann, R. Hey, and P. V. Santos, Nat. Photon. **6**, 50 (2012).

[8] P. G. Savvidis, J. J. Baumberg, R. M. Stevenson, M. S. Skolnick, D. M. Whittaker, and J. S. Roberts, Phys. Rev. Lett. **84**, 1547 (2000).

[9] R. M. Stevenson, V. N. Astratov, M. S. Skolnick, D. M. Whittaker, M. Emam-Ismail, A. I. Tartakovskii, P. G. Savvidis, J. J. Baumberg, and J. S. Roberts, Phys. Rev. Lett. **85**, 3680 (2000).

[10] J. J. Baumberg, P. G. Savvidis, R. M. Stevenson, A. I. Tartakovskii, M. S. Skolnick, D. M. Whittaker, and J. S. Roberts, Phys. Rev. B **62**, R16247 (2000).

[11] A. I. Tartakovskii, V. D. Kulakovskii, A. Forchel, and J. P. Reithmaier, Phys. Rev. B **57**, R6807 (1998).

[12] G. Dasbach, M. Schwab, M. Bayer, D. N. Krizhanovskii, and A. Forchel, Phys. Rev. B **66**, 201201(R) (2002).

[13] M. Abbarchi, V. Ardizzone, T. Lecomte, A. Lemaître, I. Sagnes, P. Senellart, J. Bloch, P. Roussignol, and J. Tignon, Phys. Rev. B **83**, 201310(R) (2011).

[14] T. Lecomte, V. Ardizzone, M. Abbarchi, C. Diederichs, A. Miard, A. Lemaitre, I. Sagnes, P. Senellart, J. Bloch, C. Delalande, J. Tignon, and P. Roussignol, Phys. Rev. B **87**, 155302 (2013).

[15] M. D. Martin, G. Aichmayr, L. Vina, and R. Andre, Phys. Rev. Lett. **89**, 077402 (2002).

[16] K. V. Kavokin, I. A. Shelykh, A. V. Kavokin, G. Malpuech, and P. Bigenwald, Phys. Rev. Lett. **92**, 017401 (2004).

[17] P. G. Lagoudakis, P. G. Savvidis, J. J. Baumberg, D. M. Whittaker, P. R. Eastham, M. S. Skolnick, and J. S. Roberts, Phys. Rev. B **65**, 161310 (2002).

[18] A. Kavokin, P. G. Lagoudakis, G. Malpuech, and J. J. Baumberg, Phys. Rev. B **67**, 195321 (2003).

[19] K. Kavokin, P. Renucci, T. Amand, X. Marie, P. Senellart, J. Bloch, and B. Sermage, Phys. Status Solidi C **2**, 763 (2005).

[20] A. Amo, T. C. H. Liew, C. Adrados, R. Houdre, E. Giacobino, A. V. Kavokin, and A. Bramati, Nat. Photon. **4**, 361 (2010).

[21] A. Kavokin, G. Malpuech, and M. Glazov, Phys. Rev. Lett. **95**, 136601 (2005).

[22] E. Kammann, T. C. H. Liew, H. Ohadi, P. Cilibrizzi, P. Tsotsis, Z. Hatzopoulos, P. G. Savvidis, A. V. Kavokin, and P. G. Lagoudakis, Phys. Rev. Lett. **109**, 036404 (2012).

[23] D. Sarkar, S. S. Gavrilov, M. Sich, J. H. Quilter, R. A. Bradley, N. A. Gippius, K. Guda, V. D. Kulakovskii, M. S. Skolnick, and D. N. Krizhanovskii, Phys. Rev. Lett. **105**, 216402 (2010).

[24] C. Adrados, A. Amo, T. C. H. Liew, R. Hivet, R. Houdré, E. Giacobino, A. V. Kavokin, and A. Bramati, Phys. Rev. Lett. **105**, 216403 (2010).

[25] C. Adrados, T. C. H. Liew, A. Amo, M. D. Martín, D. Sanvitto, C. Antón, E. Giacobino, A. Kavokin, A. Bramati, and L. Viña, Phys. Rev. Lett. **107**, 146402 (2011).

[26] S. Christopoulos, G. B. H. von Högersthal, A. J. D. Grundy, P. G. Lagoudakis, A. V. Kavokin, J. J. Baumberg, G. Christmann, R. Butté, E. Feltin, J.-F. Carlin, and N. Grandjean, Phys. Rev. Lett. **98**, 126405 (2007).

[27] D. N. Krizhanovskii, D. Sanvitto, I. A. Shelykh, M. M. Glazov, G. Malpuech, D. D. Solnyshkov, A. Kavokin, S. Ceccarelli, M. S. Skolnick, and J. S. Roberts, Phys. Rev. B **73**, 073303 (2006).

[28]G. Panzarini, L. C. Andreani, A. Armitage, D. Baxter, M. S. Skolnick, V. N. Astratov, J. S. Roberts, A. V. Kavokin, M. R. Vladimirova, and M. A. Kaliteevski, Phys. Rev. B **59**, 5082 (1999).
[29]G. Dasbach, C. Diederichs, J. Tignon, C. Ciuti, P. Roussignol, C. Delalande, M. Bayer, and A. Forchel, Phys. Rev. B **71**, 161308 (2005).
[30]J. R. Jensen, P. Borri, W. Langbein, and J. M. Hvam, Appl. Phys. Lett. **76**, 3262 (2000).
[31]R. Spano, J. Cuadra, G. Tosi, C. Antón, C. A. Lingg, D. Sanvitto, M. D. Martín, L. Viña, P. R. Eastham, M. van der Poel, and J. M. Hvam, New J. Phys. **14**, 075018 (2012).
[32]J. M. Zajac, E. Clarke, and W. Langbein, Appl. Phys. Lett. **101**, 041114 (2012).
[33]J. M. Zajac, W. Langbein, M. Hugues, and M. Hopkinson, Phys. Rev. B **85**, 165309 (2012).
[34]D. Sanvitto, A. Amo, L. Viña, R. André, D. Solnyshkov, and G. Malpuech, Phys. Rev. B **80**, 045301 (2009).
[35]E. Wertz, L. Ferrier, D. D. Solnyshkov, R. Johne, D. Sanvitto, A. Lemaitre, I. Sagnes, R. Grousson, A. V. Kavokin, P. Senellart, G. Malpuech, and J. Bloch, Nat. Phys. **6**, 860 (2010).
[36]M. Vladimirova, S. Cronenberger, D. Scalbert, K. V. Kavokin, A. Miard, A. Lemaître, J. Bloch, D. Solnyshkov, G. Malpuech, and A. V. Kavokin, Phys. Rev. B **82**, 075301 (2010).
[37]I. A. Shelykh, Y. G. Rubo, G. Malpuech, D. D. Solnyshkov, and A. Kavokin, Phys. Rev. Lett. **97**, 066402 (2006).
[38]M. M. Glazov, I. A. Shelykh, G. Malpuech, K. V. Kavokin, A. V. Kavokin, and D. D. Solnyshkov, Solid State Commun. **134**, 117 (2005).
[39]D. D. Solnyshkov, I. Shelykh, M. Glazov, G. Malpuech, T. Amand, P. Renucci, X. Marie, and A. Kavokin, Semiconductors **41**, 1099 (2007).
[40]Ł. Kłopotowski, M. D. Martín, A. Amo, L. Viña, I. A. Shelykh, M. M. Glazov, G. Malpuech, A. V. Kavokin, and R. André, Solid State Commun. **139**, 511 (2006).